Heliyon 10 (2024) e26339

Contents lists available at ScienceDirect

Heliyon

journal homepage: www.cell.com/heliyon

Research article

Synthesis of ZIF-8/$ZnFe_2O_4$/GO-OSO_3H nanocomposite as a superior and reusable heterogeneous catalyst for the preparation of pyrimidine derivatives and investigation of their antimicrobial activities

Maryam Mahdavi [a], Mohammad Ali Ghasemzadeh [a,*], Ali Javadi [b]

[a] Department of Chemistry, Qom Branch, Islamic Azad University, Qom, Iran
[b] Department of Medical Sciences, Faculty of Medicine, Qom Medical Sciences, Islamic Azad University, Qom, Iran

ARTICLE INFO

Keywords:
Graphene oxide
ZIF-8/$ZnFe_2O_4$/GO-OSO_3H
Multi-component reactions
Heterogeneous catalyst
Heterocycle
Metal-organic frameworks
Pyrimidine

ABSTRACT

In this report, we synthesized some pyrimidine derivatives by multi-component reaction of urea, benzaldehydes, and 1,3-indandione in the presence of ZIF-8/$ZnFe_2O_4$/GO-OSO_3H nanocomposite under reflux conditions. Initially, graphene oxide was prepared from graphite, and then it was sulfonated using $ClOSO_3H$. Next, GO-OSO_3H nanosheets were used to support ZIF-8/$ZnFe_2O_4$ nanostructure. The construction of the synthesized structure was established using different spectral techniques such as X-ray crystallography (XRD), scanning electron microscopy (SEM), energy dispersive X-ray spectroscopy (EDX/Mapping), Fourier transform infrared (FTIR), thermal gravimetric analysis (TGA), vibrating sample magnetometer (VSM), and Brunauer-Emmett-Teller (BET). The present method provides various benefits including the efficiency of outcomes, easy separation of the catalyst, and excellent yield of the products within short reaction times. Moreover, the antibacterial activities of pyrimidine derivatives were investigated via the agar-well diffusion method on gram-negative (*Escherichia coli*) and gram-positive (*Staphylococcus aureus*) bacteria and the obtained results illustrated reasonable effects.

1. Introduction

Heterocyclic compounds are widely distributed in nature and have biological and industrial importance. Today, many drugs contain heterocycles that are not extracted from natural sources, but synthesized in the laboratory [1]. Heterocyclic compounds are of interest to researchers due to their valuable biological actions, as well as antiviral [2], antibacterial [3], anti-inflammatory [4], antitumor [5], and antihypertensive [6]. Meanwhile, clinical properties such as antimicrobial [7], antihistamine, and antiasthmatic [8] have been described for the pyrimidine derivatives.

Metal-organic frameworks (MOFs) have captivated the consciousness of many investigators which are rapidly developing and are characterized by high porosity and abundant properties. MOFs are generally composed of metal clusters with open crystal lattices which are permanently assembled through strong cross-links [9].

Newly, utilizing MOFs as catalysts has become a new research field [10]. The diversity of MOF topologies (i.e. pores shapes and

* Corresponding author.
E-mail address: ma.ghasemzadeh@iau.ac.ir (M.A. Ghasemzadeh).

https://doi.org/10.1016/j.heliyon.2024.e26339
Received 15 August 2023; Received in revised form 11 February 2024; Accepted 12 February 2024
Available online 19 February 2024

sizes) makes MOFs attractive for a broad range of applications. The most crucial characteristic of MOFs is their high surface area. Integration of metal clusters has led to significant recovery of MOFs in porosity and stability [11]. A wide variety of MOF's structures are engineered synergistically between metal nodes, practical linkage, enclosed layers, or nanoparticles for numerous and choosy heterogeneity interplays and activates in these MOF-based nanocatalysts. The most commonly used MOFs are HKUST-1, MIL-53, Fe-BTC, UiO-66, and ZIF-8. Consequently, these materials were broadly utilized in diverse fields including drug delivery, sensing, catalyst, *etc.* [12,13].

In recent years, MIL structures have been used as catalyst in the Groebke-Blackburn-Bienaymé reaction (GBB reaction) [14], the Hantzsch synthesis [15,16], and the Biginelli reaction [17]. Moreover, the application of UiO-66 MOFs has been studied in Gewald condensation [18], pyrimido [4,5-d] pyrimidine synthesis [19,20], spirooxindoles synthesis [21], and dihydro-2-oxopyrroles synthesis [22].

One of the crucial subgroups of MOFs is the zeolitic imidazolate framework (ZIF) in which maximum series contain Co or Zn as the center of metal and imidazole imitative as connectors. ZIF-8 is the greater reviewed in the ZIFs toolbox massed from 2-methylimidazolen and Zn^{2+} [23]. ZIF structures have also played catalytic role in organic transmutations, like Friedel-Crafts acylation [24], Knoevenagel condensation [25], the synthesis of quinazolines [26], and the reduction of acetylenes [27]. In addition, the use of ZIFs has been expanded in industrial applications such as water purification from heavy metals and organic dyes [28,29], as well as the selective filtration of gaseous pollutants [30].

Magnetic nanoparticles, especially iron oxide, can rapidly bulk up. Therefore, covering the surface and supporting it through porous polymers, graphene derivatives, supramolecules, or even via other metals (neutral or noble) and oxides are the maximum common ways to protect gathering [31]. Magnetic nanoparticles are an important substrate for linking inorganic and organic catalysts. This can lead to major advances in the growth of different nanocatalytic systems via immobilizing homogeneous catalysts on magnetic nanoparticles. Magnetic nanoparticles can be also considered attached to organometallic frameworks, which provide the superiority of enhanced surface area and growth feedback rate [32].

One of the oxidized derivatives of graphene is graphene oxide (GO) which has a wide range of oxygen-containing useful groups including hydroxyl, carboxyl, and epoxy groups. Mixing GO with MOFs can exchange the distance among GO layers to have a variety of applications in GO/MOF catalysis, which can take advantage of the advisable assets of both kinds of materials and at the same time boost their physical properties. These composites increase the surface stability of MOFs and lead to new applications in various fields [33]. Pd–ZIF-8/rGO which have been used to catalyze the Knoevenagel condensation and reduce the resulting imine product [34]. Moreover, GO/Fe_3O_4/UiO-66-NH_2 was exploited in the optimal synthesis of chromene polycycles [35].

Recently, various nanostructures including rGO@Fe_3O_4@Ni [36], Fe_3O_4@GlcA@Ni-MOF [37], Cu-BTC@Fe_3O_4 [38], Fe_3O_4@P4VP@metal-organic framework [39], and MOF-5@SiO_2@Fe_3O_4 [40] have been used as catalyst in organic reactions. Although these reported nanocomposites have efficient catalytic activity and enjoy high stability, high surface area, high yields, and easy long-term reusability, however, intrinsic functionalities of substrates can be exploited as easy anchoring sites for nanocomponents.

Gram-negative and Gram-positive bacteria are classified based on their cell wall structure and response to Gram staining. Gram-negative bacteria such as Escherichia coli *have a thin layer of peptidoglycan in their cell wall that is surrounded by an outer membrane containing lipopolysaccharides, which makes them more resistant to some antibiotics. When stained with a warm stain, they appear pink or red under the microscope. On the other hand, Gram-positive bacteria such as Staphylococcus aureus have a thick layer of peptidoglycan in their cell wall, but they lack an outer membrane, which makes them more sensitive to antibiotics, and antibiotics easily penetrate the cell wall. When stained with warm stain, they appear purple or blue under the microscope* [41,42].

The incorporation of the merits of MOFs and GO to construct a novel class of composites with both enhanced functionality and large surface area is of great significance and interest. Recently, nanotechnology with a wide diversity of nanomaterials has created a new revolution in science and especially in chemical fields [43–48].

This study, considering the importance of heterogeneous catalysts based on graphene oxide, ZIF-8, and magnetic nanoparticles, is intended to produce ZIF-8/$ZnFe_2O_4$/GO-OSO_3H nanocomposite as a robust and reusable catalyst for the production of pyrimidine derivatives (Scheme 1). In addition, the antibacterial activities of pyrimidine derivatives were investigated via agar-well diffusion method on gram-negative (*Escherichia coli*) and gram-positive (*Staphylococcus aureus*) bacteria that showed satisfactory consequences.

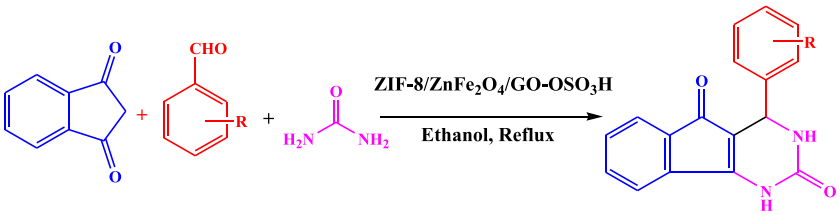

Scheme 1. Synthesis of pyrimidines using ZIF-8/$ZnFe_2O_4$/GO-OSO_3H as catalyst.

2. Experimental

2.1. Materials and analysis

The high-purity chemicals were bought from Sigma-Aldrich and Merck. The substances with the commercial reagent grades were utilized without further purification. The melting point was unmodified and defined in a capillary tube over a melting point microscope (Boetius). ^{1}H NMR and ^{13}C NMR spectra were attained on Bruker 250 MHz spectrometer with $CDCl_3$ as a solvent and TMS as an internal standard. Recording FT-IR spectra was performed on Magna-IR, spectrometer 550. Powder XRD (X-ray diffraction) was performed on a Philips diffractometer (X'pert Co.) with Cu Kα mono chromatized radiation (λ = 1.5406 Å). The microscopic morphology of the products was observed through SEM (LEO, 1455VP). The energy dispersive analysis of X-ray was used to perform compositional analysis (EDX, Kevex, Delta Class 1). A Mettler Toledo TGA was considered to perform thermogravimetric analysis (TGA) under argon, and heating was performed to 825 °C from room temperature. A Belsorp mini automatic adsorption tool was used to measure nitrogen adsorption-desorption isotherms at 196 °C followed by degassing the specimens for 5 h at 150 °C. The sample weight was estimated at 10 mg in the TG test with heating at 10 °C per minute. To analyze the magnetometer, the vibrating sample (VSM) was examined using a device (MDKFD) at room temperature.

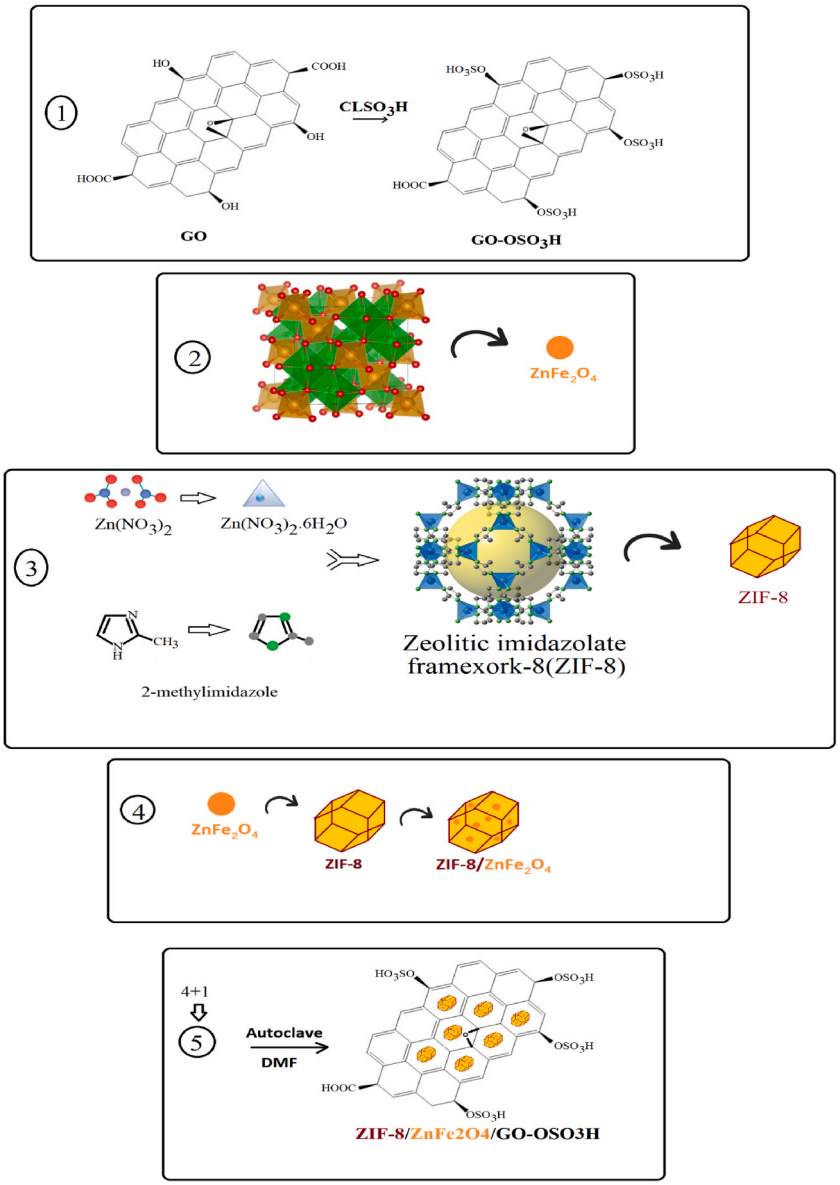

Scheme 2. The preparation steps of ZIF-8/$ZnFe_2O_4$/GO-OSO_3H nanocatalyst.

2.2. Synthesis of graphene

In this study, graphene was prepared using graphite, $KMNO_4$, and H_2SO_4 via the modified Hummer's method [49].

2.3. Preparation of graphene oxide

GO was made via the modified Hummer's method, as follows: sodium nitrate (2.5 g) and graphene (5 g) were put in sulfuric acid (115 mL, 98%), and the solution was set down on a magnetic stirrer provided with a condenser put in an ice bath. In continuation, $KMnO_4$ (15 g) was added steadily over 120 min. The reaction mixture was then put in a water bath (35 °C) and mixed for 30 min. Then, 230 mL of deionized water was slowly poured into the vessel, and the mixture was kept at 98 °C for 15 min. To terminate the reaction, 700 mL of deionized water and H_2O_2 (50 mL, 30%) were consequently poured into the solution. When the reaction was complete, the residue was cleaned with deionized water and HCl (5%) three times. The gained GO was then dried at 60 °C for 12 h [50].

2.4. Synthesis of sulfonated GO

GO (1 g) was distributed in chloroform for 1 h and then chlorosulfonic acid was poured into the dispersed solution. The solution was then refluxed for 4 h at 60 °C in a round-bottomed flask via a cold-water condenser. Finally, the cooled suspension was filtered and washed with excess ethanol to afford sulfonated graphene oxide (Step 1, Scheme 2) [51].

2.5. Preparation of $ZnFe_2O_4$ nanoparticles

Initially, $FeCl_3.6H_2O$ (0.2 M) and $ZnCl_2.6H_2O$ (0.1 M) were dissolved individually in 75 mL of distilled water. Next, NaOH (2 M) was poured dropwise into the $FeCl_3$ solution till the pH of the solution reached 10. Then, the $ZnCl_2$ solution was added to another mixture. Next, the temperature of the reaction was increased to 80 °C for 3 h to produce a brown residue. The earned residue was washed several times with distilled water and ethanol via centrifugation, and then kept at room temperature for 24 h. Finally, $ZnFe_2O_4$ nanoparticles were obtained in the furnace at 500 °C for 5 h (Step 2, Scheme 2) [52].

2.6. Preparation of ZIF-8

6.5 g of 2-methylimidazole was dispersed in 80 mL of methanol. Then, $Zn(NO_3)_2.6H_2O$ solution (0.25 M) was added to 2-methylimidazole solution under vigorous stirring at room temperature for 24 h. The obtained solid was then collected via centrifugation and washed with methanol for five times. Eventually, the achieved product dried at 75 °C under vacuum (Step 3, Scheme 2) [53].

2.7. Synthesis of ZIF-8/$ZnFe_2O_4$

A mixture of ZIF-8 (0.2 g) and $ZnFe_2O_4$ (0.1 g) was mixed in methanol (20 mL), and the mixture was placed in an autoclave at 100 °C for 24 h. The final precipitate was washed twice with DMF and methanol and then dried overnight at room temperature (Step 4, Scheme 2) [54].

2.8. Preparation of ZIF-8/$ZnFe_2O_4$/GO-OSO_3H

Initially, sulfonated GO (0.5 g) and ZIF-8/$ZnFe_2O_4$ (1.1 g) were dispersed in 30 mL of DMF. Then, it was placed in an autoclave at a temperature of 120 °C for 12 h. Afterward, the obtained sediment was washed twice with DMF and methanol. Finally, the produced ZIF-8/$ZnFe_2O_4$/GO-OSO_3H was dried at 40 °C for 24 h (Step 5, Scheme 2) [55].

The preparation steps of ZIF-8/$ZnFe_2O_4$/GO-OSO_3H nanocatalyst are shown in Scheme 2.

2.9. The preparation method for the synthesis of pyrimidine derivatives

To synthesize pyrimidine derivatives, a mixture of 1,3-indanedione (0.5 mmol), urea (1.5 mmol), arylaldehyde (0.5 mmol), and ZIF-8/$ZnFe_2O_4$/GO-OSO_3H (0.005 g) was stirred in ethanol as solvent (7 mL) for about 30 min. The reaction progress was monitored by TLC (n-hexane: ethyl acetate 5: 1). After completion of the reaction, the heterogeneous catalyst was separated via a magnet, and then the resultant precipitate was filtered and recrystallized from ethanol and dried for 12 h. The spectral data of new products are shown below.

4- Cyano -3,4-dihydro-1H-indeno [1,2-d] pyrimidine-2,5-dione (4i): $C_{18}H_{11}N_20_2$:^{1}H NMR (300 MHz, $CDCl_3$) δ: 5.49 (s, 1H, –CH), 7.19 (s, 1H, NH), 8.44 ppm (s, 1H, NH),7.2–8.4 (m, 8H, H_{Ar}); ^{13}C NMR (62.9 MHz, $CDCl_3$) δ: 41.22, 115.28, 118.26, 123.66, 123.70, 131.83, 132.2, 132.90, 133.72, 135.88, 135.99, 136.71, 140.19, 142.55, 143.31, 188.49, 189.21; FT-IR (KBr):1589 (C═C), 1693 (C═O), 1724 (C═O), 2225 (CN), 3437 (NH) cm^{-1}.

2- Methoxy -3,4-dihydro-1H-indeno [1,2-d] pyrimidine-2,5-dione (4j): $C_{18}H_{14}N_20_3$: ^{1}H NMR (300 MHz, $CDCl_3$) δ: 3.07 ppm (s, 3H, OCH_3), 5.13 (s, 1H, CH), 7.74 (s,1H, NH), 8.44 (s, 1H, NH), 6.96–8.89 (m,8H, H_{Ar}); ^{13}CNMR (62.9 MHz, $CDCl_3$) δ: 38.89, 55.79, 105.02, 110.69, 120.42, 122.05, 123.22, 128.29, 133.99, 135.05, 135.71, 135.42, 140.11, 141.43, 142.42, 160.56, 189.33, 190.68; FT-IR (KBr): 1684 (C═O), 1705 (C═O), 3425 (NH) cm^1.

2-Hydroxy, 4-Fluoro-3,4-dihydro-1H-indeno [1,2-d]pyrimidine-2,5-dione (4k): $C_{17}H_{11}N_2O_2F$: ^{1}H NMR (300 MHz, $CDCl_3$) δ: 5.75 ppm (s,1H, CH), 7.20–7.83 (m,7H, H_{Ar}), 9.00 (s, 1H, NH), 9.20 (1H, NH), 10.20 (1H,OH); ^{13}CNMR (62.9 MHz, $CDCl_3$) δ: 37.7, 38.3, 112.1, 114.9, 117.1, 126.0, 129.6, 129.7, 131.2, 135.0, 137.4, 138.9, 139.3, 151.5, 154.5, 186.0; FT-IR (KBr): 1590 (C═O), 1701 (C═O), 3170 (NH), 3407 (OH) cm^{-1}.

2- Hydroxy, 4-Bromo-3,4-dihydro-1H-indeno [1,2-d]pyrimidine-2,5-dione (4l): $C_{17}H_{11}N_2O_2Br$: ^{1}H NMR (300 MHz, $CDCl_3$) δ: 5.70 ppm (s, 1H, CH), 9.00 (s, 1H, NH), 9.20 (1H, NH), 10.0 (s, 1H,OH), 7.20–7.83 (m,7H, H_{Ar}); ^{13}CNMR (62.9 MHz, $CDCl_3$) δ: 37.6, 37.7, 112.1115.5, 117.1, 126.0, 129.6, 129.7, 131.2, 131.8, 134.2, 137.4, 138.9, 140.01, 154.9, 156.8, 187.0; FT-IR (KBr): 1600 (C═O), 1715 (C═O), 2950 (NH), 3402 (OH) cm^{-1}.

2.10. Evaluation of antibacterial activity

The antibacterial activity of the prepared products was evaluated using well diffusion method on Mueller-Hinton Agar (MHA). Inhibitory zones were reported in millimeters. *S. aureus* (ATCC 25923) and *E. Coli* (ATCC 25922) were used as references for the antibacterial assay of the products. In addition, gentamicin was used as a positive standard. Briefly, MHA plates were inoculated with a bacterial strain under aseptic conditions. All the compounds were prepared with a concentration of 512 μg/mL in the solvent and antibacterial tests of the compounds were performed according to CLSI standards [56], and incubated at 37 °C for 24 h. After the incubation period, the diameter of growth inhibition zones was measured.

3. Results and discussion

3.1. FT-IR spectroscopy

The structure of ZIF-8/$ZnFe_2O_4$/GO-OSO_3H was considered via FT-IR spectroscopy (Fig. 1). As shown, the peak at 3428 cm^{-1} is due to the stretching vibration of OH groups in the structure [57]. The peak at 2923 cm^{-1} is due to the C–H stretch of imidazole groups [58], and at 2853 cm^{-1} stretching vibration of the C–H bond appears [59]. Moreover, the peak at 1632 cm^{-1} corresponds to the tensile vibration of the groups of carbonyl located at the edging of GO, while the adsorption band at 1484 cm^{-1} is due to the C═N bond in the imidazole ring. In addition, the peaks at 1384 cm^{-1}, 1156 cm^{-1} are related to the stretching vibration of C–O and S═O bonds, respectively [60]. Moreover, the peaks at 757 cm^{-1}, and 616 cm^{-1} are relevant to the Zn–N and Zn–O bonds [61], and the peak at 458 cm^{-1} is relevant to the Fe–O.

3.2. SEM analysis

Field emission scanning electron microscopy (SEM) is a useful technique for determining the size distribution of particles and porosity. The morphology and size of the ZIF-8/$ZnFe_2O_4$/GO-OSO_3H particles were determined using SEM are shown in Fig. 2. The results indicate that the prepared nanostructure exhibits a uniform particle shape with a particle size ranging from 71 to 85 nm (Fig. 2a and b).

3.3. BET analysis

Brunauer-Emmett-Teller (BET) analysis (Fig. 3a), adsorption/desorption (Fig. 3b), and BJH analysis (Fig. 3c) of the ZIF-8/$ZnFe_2O_4$/GO-OSO_3H nanocomposite are illustrated in Fig. 3. The average diameter of the pores of the nanocatalyst is 1.21 nm, which shows the presence of porosity on the nanoscale. The analysis isotherm for ZIF-8/$ZnFe_2O_4$/GO-OSO_3H is more consistent with the type

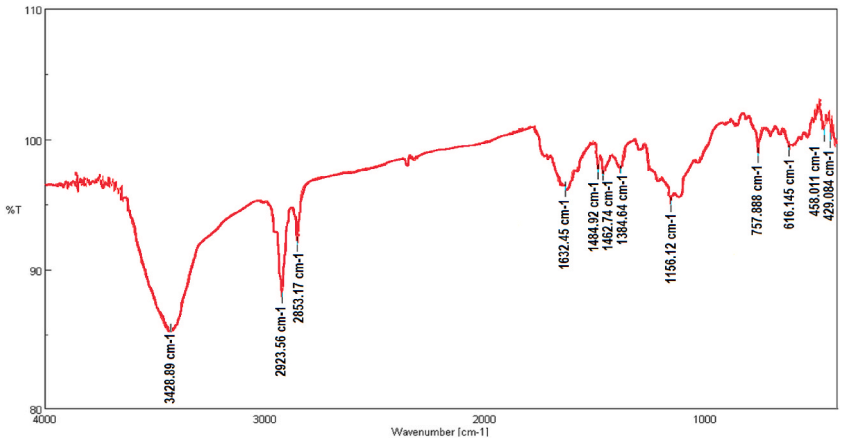

Fig. 1. FT-IR spectrum of ZIF-8/$ZnFe_2O_4$/GO-OSO_3H.

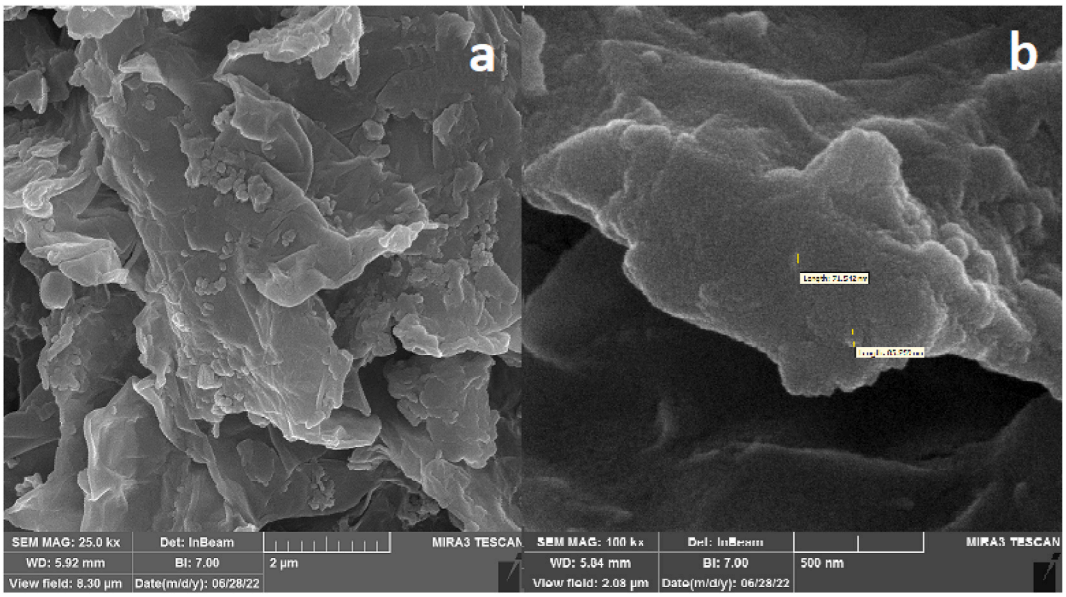

Fig. 2. The SEM images of ZIF-8/$ZnFe_2O_4$/GO-OSO_3H (Fig. 2a and b) with various magnifications.

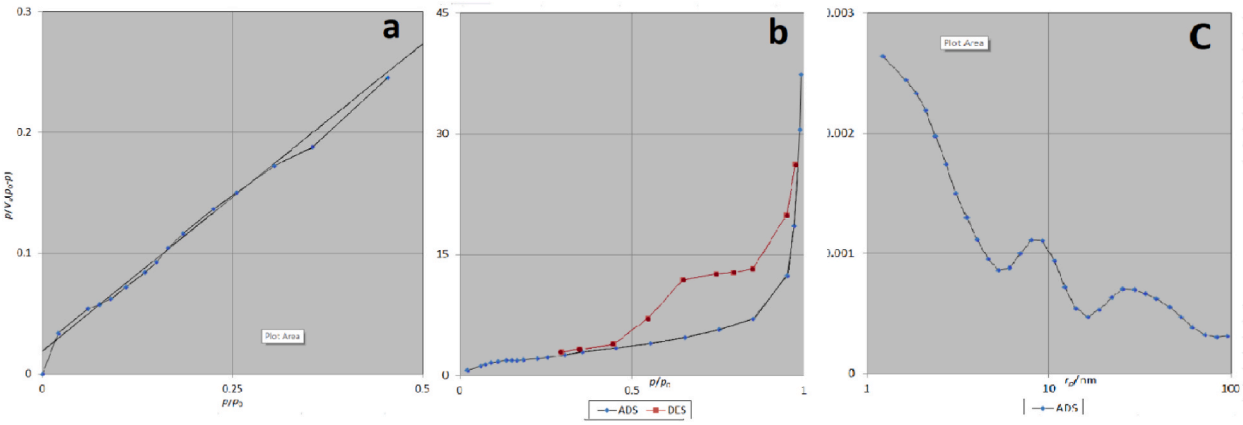

Fig. 3. BET analysis (a), adsorption/desorption (b), and BJH analysis (c) of ZIF-8/$ZnFe_2O_4$/GO-OSO_3H nanocomposite.

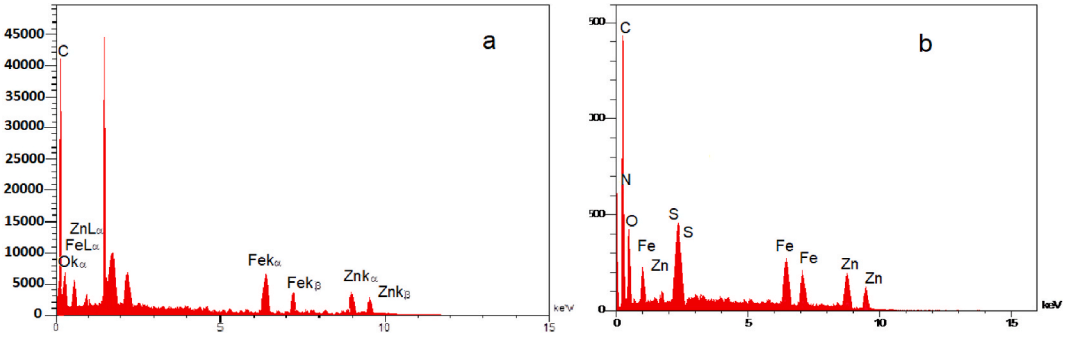

Fig. 4. EDX spectra of ZIF-8/$ZnFe_2O_4$ (a), and ZIF-8/$ZnFe_2O_4$/GO-OSO_3H (b).

I adsorption isotherm, which confirms the pore volume distribution in the fine range. Also, the pore volume of the cavities in the ZIF-8/$ZnFe_2O_4$/GO-OSO_3H was calculated to be 1.8928 $cm^{-3}g^{-1}$, which was constant through the literature [62].

3.4. EDX analysis

The chemical Purity of the samples experimented with utilizing energy-dispersive X-ray spectroscopy (EDX). Fig. 4a–b shows the EDX spectra of ZIF-8/$ZnFe_2O_4$ and ZIF-8/$ZnFe_2O_4$/GO-OSO_3H, respectively. As illustrated, ZIF-8/$ZnFe_2O_4$ has only O, Zn, C, and Fe elements, and in Fig. 4b the elements including Fe, Zn, O, S, and C were observed for ZIF-8/$ZnFe_2O_4$/GO-OSO_3H. In addition, EDX examination has been accomplished in an elemental mapping manner on ZIF-8/$ZnFe_2O_4$/GO-OSO_3H nanocomposite (Fig. 5). The highly dispersed distribution of elements confirmed that there were no impurities in the produced nanocomposite. It was concluded that all of the elements including Zn (Fig. 5a), C (Fig. 5b), Fe (Fig. 5c), S (Fig. 5d), N (Fig. 5e), O (Fig. 5f), and all elements (Fig. 5g) were verified by EDX-mapping analysis. The obtained results exhibit superb purity and homogeneous dispersion. Fig. 5g illustrates the homogeneous arrangement of components all-round the structure.

3.5. XRD analysis

The analysis of X-ray diffraction (XRD) for ZIF-8/$ZnFe_2O_4$/GO-OSO_3H is shown in Fig. 6. Diffraction peaks at 33°, 35°, and 62° are related to the crystalline structure of $ZnFe_2O_4$ [63]. According to the literature, the peaks at 12.5°, 18° are correspond to ZIF-8, and the related peak of GO-OSO_3H at 14° overlaps with very strong peaks related to Zn. Moreover, the presence of OSO_3H groups prevents GO peaks from appearing well. It can also be assumed that GO-OSO_3H nanosheets are grouped by $ZnFe_2O_4$ nanoparticles in the 20–30° section [64].

3.6. TGA analysis

Thermogravimetric analysis (TGA) shows that the ZIF-8/$ZnFe_2O_4$/GO-OSO_3H sample has three weight loss regions at 100–800 °C, indicating the organometallic nature of the structure (Fig. 7). The first one at 0–100 °C is connected to the deprivation of solvents from the frame. Loss weight for the second stage is in the range of 200–500 °C, illustrating the decomposition of the structure of ZIF-8 because of the decomposition of the metal-organic framework [65]. Finally, the observed degradation at 500–800 °C can be attributed to the destruction of GO-OSO_3H [66–69].

3.7. VSM analysis

Vibrating sample magnetometers (VSM) for ZIF-8/$ZnFe_2O_4$ and ZIF-8/$ZnFe_2O_4$/GO-OSO_3H samples are shown in Fig. 8. As observed, the saturation magnetization of ZIF-8/$ZnFe_2O_4$ is about 0.07 emu/g (Fig. 8a), and the saturation magnetization of ZIF-8/$ZnFe_2O_4$/GO-OSO_3H is 0.05 emu/g (Fig. 8b). It has been concluded that GO-OSO_3H is non-magnetic, and when it is added, the magnetic property decreases.

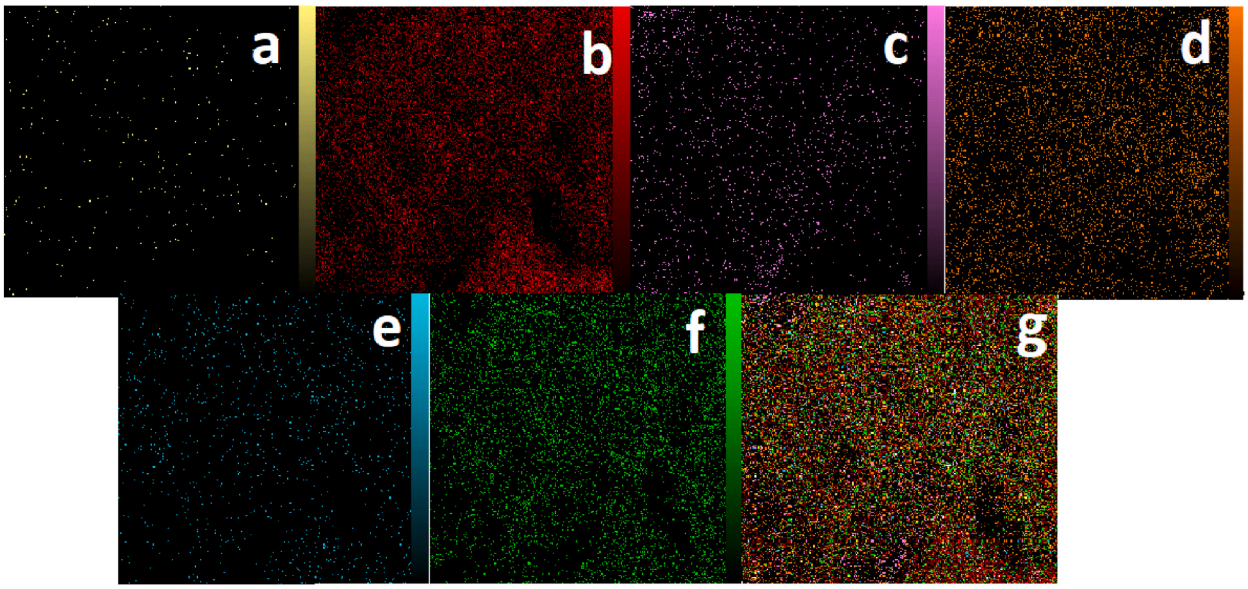

Fig. 5. EDX-Mapping of ZIF-8/$ZnFe_2O_4$/GO-OSO_3H; Zn (Fig. 5a), C (Fig. 5b), Fe (Fig. 5c), S (Fig. 5d), N (Fig. 5e), O (Fig. 5f), and all elements (Fig. 5g).

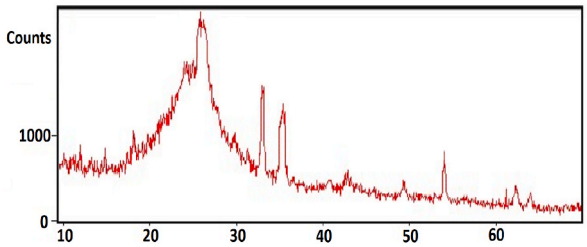

Fig. 6. The XRD pattern of ZIF-8/$ZnFe_2O_4$/GO-OSO_3H.

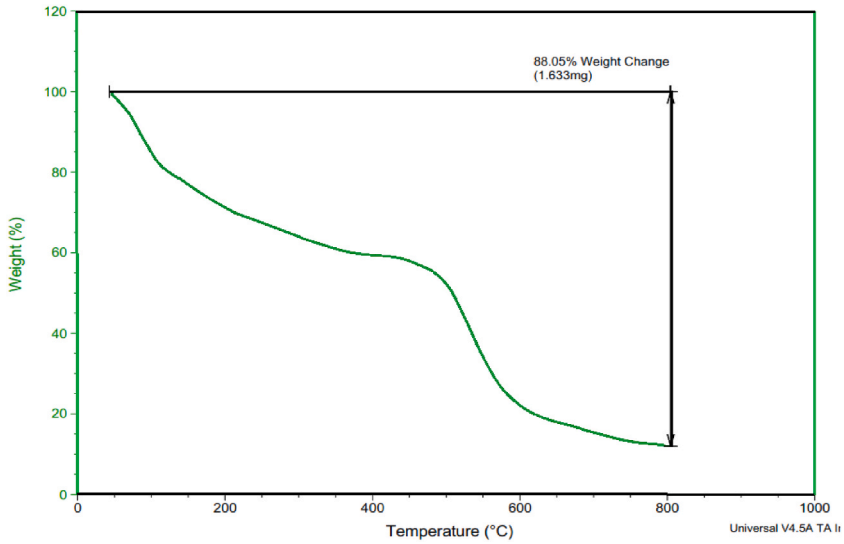

Fig. 7. TGA analysis of ZIF-8/$ZnFe_2O_4$/GO-OSO_3H.

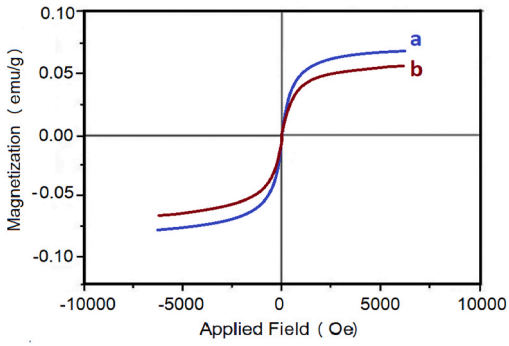

Fig. 8. VSM analysis of ZIF-8/$ZnFe_2O_4$ (a), ZIF-8/$ZnFe_2O_4$/GO –OSO_3H (b).

3.8. Optimization of reaction conditions

In this research, by selecting the model reaction using 1,3-Indandione, 4 cyano-benzaldehyde, and urea, different conditions including solvents, temperatures, and catalysts were investigated. As shown in Table 1, different solvents such as H_2O, EtOH, H_2O/EtOH (1:1), DMF, CH_3CN, and $PhCH_3$ along with solvents-free conditions at different temperatures using ZIF-8/$ZnFe_2O_4$/GO-OSO_3H were evaluated. As illustrated, the best results were obtained in the attendance of ethanol as solvent under reflux conditions (Table 1).

After optimizing the reaction conditions, to compare our prepared catalyst with other catalysts, the model reaction was conducted by diverse catalysts that had acidic or basic properties. The results are shown in Fig. 9. In the investigation of different catalysts, 0.01 g of each catalyst was used, and the accomplishment of the reaction was checked via TLC. The best performance corresponded to the ZIF-8/$ZnFe_2O_4$/GO-OSO_3H catalyst, which has several acidic sites in its structure.

Table 1
The model reaction optimization in different solvents and temperatures using ZIF-8/$ZnFe_2O_4$/GO-OSO_3H nanocatalyst.

Entry	solvents	Temp. (°C)	Time (min)	Yield[a] (%)
1	–	25	240	50
2	–	70	180	60
3	–	80	180	60
4	–	100	180	70
5	H_2O	70	180	65
6	CH_3CN	Reflux	160	60
7	H_2O	Reflux	180	60
8	**EtOH**	**Reflux**	**45**	**98**
9	DMF	Reflux	60	90
10	$PhCH_3$	Reflux	360	45

[a] Isolated Yield.

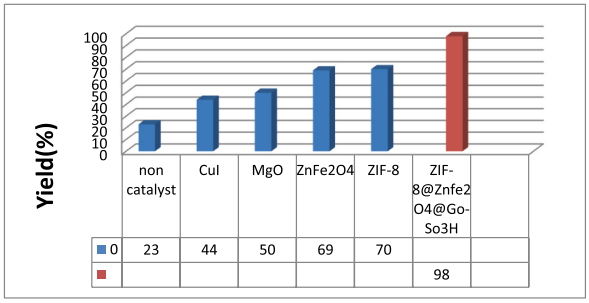

Fig. 9. The effect of various catalysts and the absence of a catalyst on the model reaction.

To evaluate the effectiveness of the catalyst, a comparison was made in the model reaction in the presence or the absence of the ZIF-8/$ZnFe_2O_4$/GO-OSO_3H catalyst with different amounts, including 0–0.007 g. As illustrated, the proper amount of the catalyst was 0.005 g with an efficiency of 98% yield in 45 min (Fig. 10).

In the continuation of our study, we decided to examine diverse benzaldehydes to evaluate the catalytic activity of ZIF-8/$ZnFe_2O_4$/GO-OSO_3H in the synthesis of pyrimidine derivatives. As expected, aryl aldehydes with electron-withdrawing groups give rise to higher yields and shorter reaction times than aldehydes with electron-donating groups (Table 2). The advantages of this research are include high efficiency, mild reaction conditions, the catalyst's reusability, and a short duration.

3.9. Reusing and recycling the catalyst

The recyclability of the ZIF-8/$ZnFe_2O_4$/GO-OSO_3H catalyst was investigated under the optimal conditions of the model study. As shown in Fig. 11, due to the heterogeneity and magnetic properties of the catalyst, it was simply divided from the crude via an external magnet and used for six cycles.

3.10. The proposed reaction mechanism

The proposed mechanism, based on the present study and previous literature [70], for the synthesis of pyrimidine derivatives

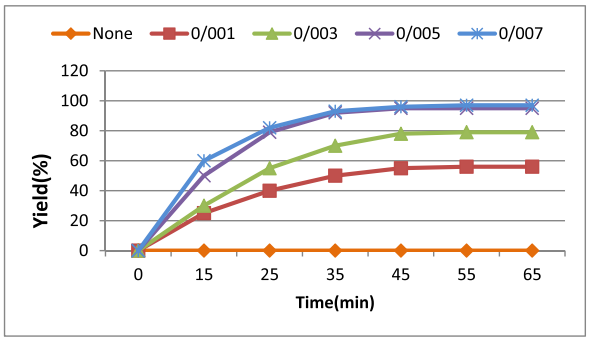

Fig. 10. The optimization of the catalyst amount for the synthesis of the corresponding pyrimidine.

Table 2
Synthesis of pyrimidine derivatives with benzaldehyde derivatives, using ZIF-8/$ZnFe_2O_4$/GO-OSO_3H as a catalyst
*Compounds 4i, 4j, 4k, and 4l are new products.

Entry	ArCHO	Product	Time (min)	Yield (%)	m.p. (°C)
4a	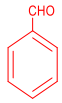	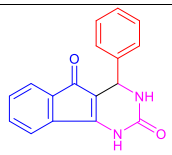	60	95	175-178 [70,71]
4b		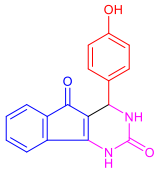	60	90	250-255[69-70]
4c		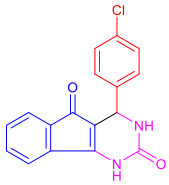	45	94	215-217[71]
4d		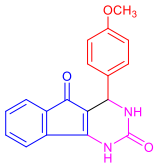	45	92	204-206[70]
4e		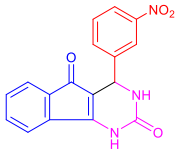	60	90	200-204[69]
4f		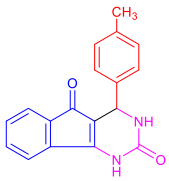	60	92	200-202[70]
4g	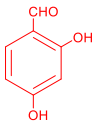	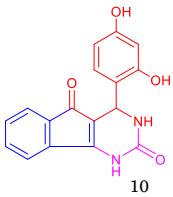	60	90	196-200[70]

4h	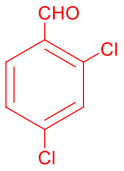	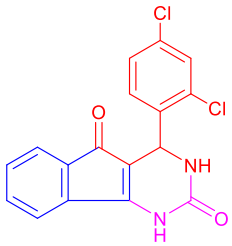	45	92	184-186[70]
4i*		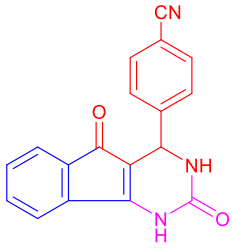	45	98	202-204
4j*	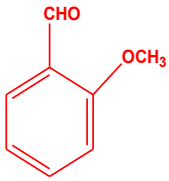	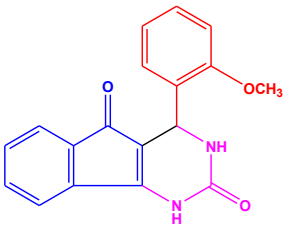	63	90	205-210
4k*	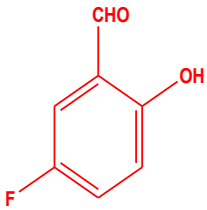	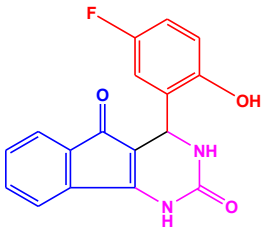		90	200-205
4l*	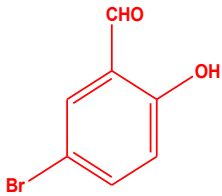	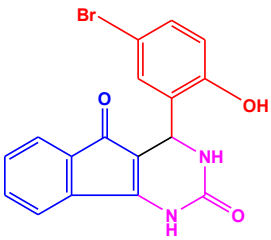	50	90	200-205

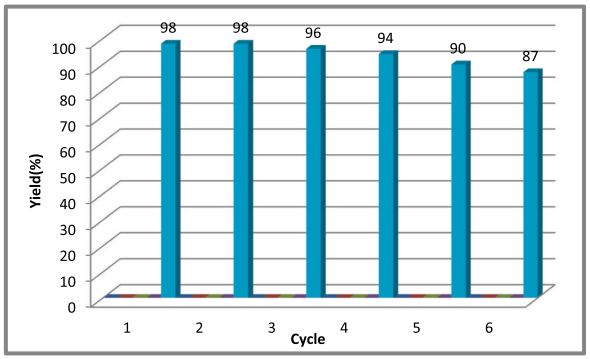

Fig. 11. The reusability of ZIF-8/$ZnFe_2O_4$/GO-OSO_3H catalyst.

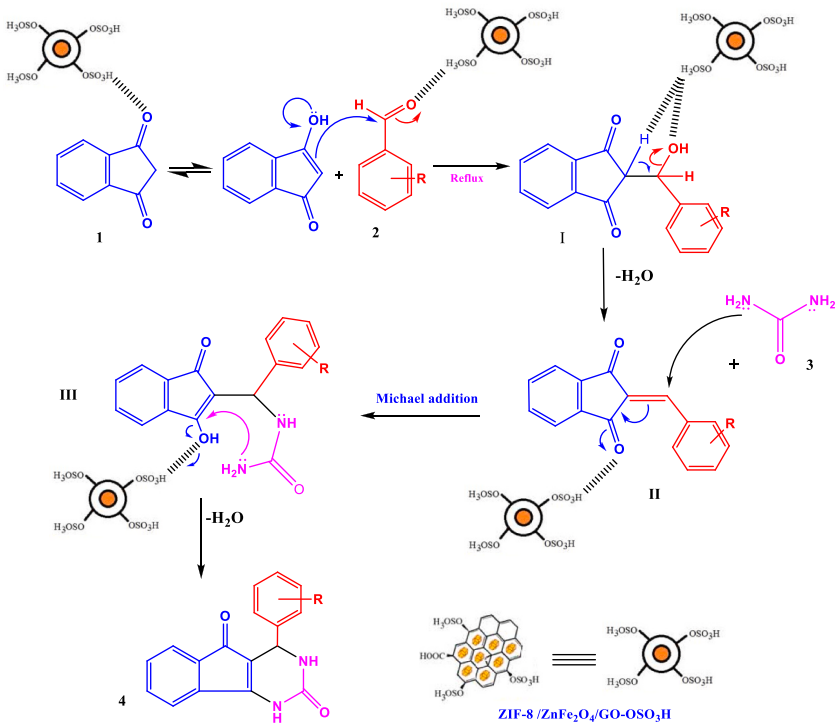

Scheme 3. Proposed mechanism for the synthesis of Pyrimidine derivatives using ZIF-8/$ZnFe_2O_4$/GO-OSO_3H.

catalyzed by ZIF-8/$ZnFe_2O_4$/GO-OSO_3H is shown in Scheme 3. It is presumed that $ZnFe_2O_4$ and ZIF-8 act as Lewis acids which increase the electrophilicity of the carbonyl groups of the aldehyde and 1,3-indanedione through a strong coordination bond [71,72]. The reaction proceeds via condensation of 1,3-indanedione 1 via aryl aldehyde 2 to yield intermediate I. Dehydration of the intermediate I, followed by the Michael addition of urea, led to the formation of intermediate II. In the end, the intermediate III goes through a process called intramolecular cycloaddition to make product 4.

3.11. Results of antimicrobial activities

The inhibition zone diameter was evaluated via evaluation of antimicrobial activities (Fig. 12). Antibacterial test results were included for compounds (4a-4j) by *Staphylococcus aureus* bacterium (Fig. 12a), and also for compounds (4a-4j) using *Escherichia coli* bacterium (Fig. 12b). The diameter of the inhibition zone for the synthesized pyrimidines against *Staphylococcus aureus* and *Escherichia coli* bacteria is depicted in Table 3.

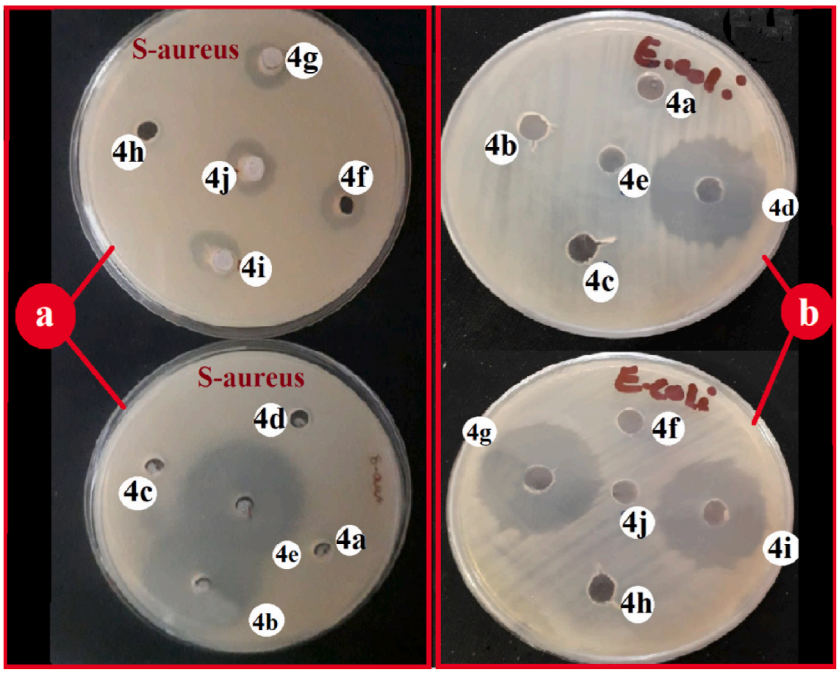

Fig. 12. The antibacterial test results including *Staphylococcus aureus* (a), and *Escherichia coli* (b) bacteria.

Table 3
The antibacterial activities of pyrimidine derivatives.

Product	*S. aureus* (mm) (ATTCC-25923)	*E. coli* (mm) (ATTCC-25922)
4a	-	-
4b	36	–
4c	–	–
4d	-	24
4e	40	-
4f	13	-
4 g	13	23
4h	–	–
4i	15	25
4j	15	-

4. Conclusion

In this study, a reasonable synthesis method for the preparation of pyrimidine compounds using ZIF-8/$ZnFe_2O_4$/GO-OSO_3H as an efficient catalyst is reported. The acidic nature of the catalyst makes it more efficient and less time-consuming, with excellent yields in comparison with other catalysts. The properties of the produced heterogeneous catalyst were examined via different methods, including EDS, SEM, BET, TGA, VSM, XRD, and FT-IR analysis. The catalyst was simply retrieved and reused for six cycles without any notable loss of its catalytic activity. The antibacterial attributes of pyrimidines were considered via the agar-well diffusion technique on gram-negative (*E.*m*coli*) and gram-positive (*S. aureus)* bacteria which demonstrated appropriate results. Utilization of this catalyst is suggested as a green and reasonable method for the synthesis of pyrimidine derivatives under green reaction conditions.

CRediT authorship contribution statement

Maryam Mahdavi: Methodology, Investigation, Data curation. **Mohammad Ali Ghasemzadeh:** Writing – review & editing, Writing – original draft, Visualization, Validation, Supervision, Resources, Project administration, Funding acquisition, Formal analysis, Conceptualization. **Ali Javadi:** Visualization, Supervision, Data curation.

Declaration of competing interest

The authors declare that they have no known competing financial interests or personal relationships that could have appeared to

influence the work reported in this paper.

Acknowledgements

The Financial Support was provided by the Research Affairs Office of the Islamic Azad University, Qom Branch, Qom, I. R. Iran [grant number 2019-2898].

References

[1] A.U. Czaja, N. Trukhan, U. Müller, Industrial applications of metal–organic frameworks, Chem. Soc. Rev. 38 (2009) 1284–1293.
[2] C.O. Kappe, Highly versatile Solid phase synthesis of biofunctional 4-aryl-3,4-dihydropyrimidines using resin-bound isothiourea building blocks and multidirectional resin cleavage, Bioorg. Med. Chem. Lett. 10 (2000) 49–51.
[3] A.D. Patil, N. V Kumar, W. C Kokke, M.F. Bean, A.J. Freyer, C. D Brosse, B. Carte, Novel alkaloids from the sponge batzella sp.: inhibitors of HIV gp120-human CD_4 binding, J. Org. Chem. 60 (1995) 1182–1188.
[4] E. Palaska, G. Şahin, P. Kelicen, N.T. Durlu, G. Altinok, Synthesis and anti-inflammatory activity of 1-acylthiosemicarbazides, 1,3,4-oxadiazoles, 1,3,4-thiadiazoles and 1,2,4-triazole-3-thiones. Il Farmaco (2002) 101–107.
[5] Gary J. Grover, Steven Dzwonczyk, Diane M. McMullen, Diane E. Normandin, Charles S. Parham, Paul G. Sleph, Suzanne Moreland, Pharmacologic profile of the dihydropyrimidine calcium channel blockers SQ 32,547 and SQ 32,946, J. Cardiovasc. Pharmacol. 26 (1995) 289–294.
[6] C. Oliver Kappe, 100 years of the biginelli dihydropyrimidine synthesis, Tetrahedron 49 (1993) 6937–6963.
[7] M.A. Ghasemzadeh, J. Safaei-Ghomi, An efficient, one-pot synthesis of polyfunctionalised dihydropyridines catalysed by AgI nanoparticles, J. Chem. Res. 38 (2014) 313–316.
[8] M. Marinescu, Biginelli reaction mediated synthesis of antimicrobial pyrimidine derivatives and their therapeutic properties, Molecules 26 (2021) 6022.
[9] K.C. Kim, Design strategies for metal-organic frameworks selectively capturing harmful gases, J. Organomet. Chem. 854 (2018) 94–105.
[10] L. Jiao, Y. Wang, H.L. Jiang, Q. Xu, Metal-organic frameworks as platforms for catalytic appliations, Adv. Mater. 30 (2017) 37.
[11] M.S. Denny, J.C. Moreton, L. Benz, S.M. Cohen, Metal–organic frameworks for membrane-based separations, Nat. Rev. Mater. 1 (2016) 12.
[12] A.J. Howarth, A.W. Peters, N.A. Vermeulen, T. C Wang, J.T. Hupp, O.K. Farha, "Best practices for the synthesis, activation, and characterization of metal–organic frameworks, Chem. Mater. 29 (2016) 26–39.
[13] S. Bibi, E. Pervaiz, M. Ali, Synthesis and applications of metal oxide derivatives of ZIF-67: a mini-review, Chem. Pap. 75 (2021) 2253–2275.
[14] A. Shaabani, H. Sepahvand, M.M. Amini, A. Hashemzadeh, M. Borjian Boroujeni, E. Badali, Tandem oxidative isocyanide-based cycloaddition reactions in the presence of MIL-101(Cr) as a reusable solid catalyst, Tetrahedron 74 (2018) 1832–1837.
[15] S. Rostamnia, H. Alamgholiloo, M. Jafari, Ethylene diamine post-synthesis modification on open metal site Cr-MOF to access efficient bifunctional catalyst for the Hantzsch condensation reaction, Appl. Organomet. Chem. 32 (2018) 4370–4379.
[16] S. Babaee, M. Zarei, H. Sepehrmansourie, M.A. Zolfigol, S. Rostamnia, Synthesis of metal–organic frameworks MIL-101(Cr)-NH_2 containing phosphorous acid functional groups: application for the synthesis of N-Amino-2-pyridone and pyrano [2,3-c]pyrazole derivatives via a cooperative vinylogous anomeric-based oxidation, ACS Omega 5 (2020) 6240–6249.
[17] H. Sepehrmansouri, M. Zarei, M.A. Zolfigol, A.R. Moosavi-Zare, S. Rostamnia, S. Moradi, Multilinker phosphorous acid anchored En/MIL-100(Cr) as a novel nanoporous catalyst for the synthesis of new N-heterocyclic pyrimido[4,5-b]quinolines, Mol. Catal. 481 (2020) 110303–110320.
[18] N. Erfaninia, R. Tayebee, M. Dusek, M.M. Amini, Ethylene diamine grafted nanoporous UiO-66 as an efficient basic catalyst in the multi-component synthesis of 2-aminithiophenes, Appl. Organomet. Chem. 32 (2018) 4307–4317.
[19] R. Ghorbani-Vaghei, D.A. Davood Azarifar, S. Daliran, A.R. Oveisi, The UiO-66-OOSO3H metal–organic framework as a green catalyst for the facile synthesis of dihydro-2-oxypyrrole derivatives, RSC Adv. 6 (2016) 29182–29189.
[20] Z. Mahmoudi, M.A. Ghasemzadeh, H. Kabiri-Fard, Fabrication of UiO-66 nanocages confined brønsted ionic liquids as an efficient catalyst for the synthesis of dihydropyrazolo[4′,3′:5,6]pyrano[2,3-d]pyrimidines, J. Mol. Struct. 1194 (2019) 1–10.
[21] B. MirhosseiniEshkevari, M.A. Ghasemzadeh, M. Esnaashari, Highly efficient and green approach for the synthesis of spirooxindole derivatives in the presence of novel Brønsted acidic ionic liquids incorporated in UiO-66 nanocages, Appl. Organomet. Chem. 33 (2019) 5027–5040.
[22] A. Shaabani, R. Mohammadian, S.E. Hooshmand, A. Hashemzadeh, M.M. Amini, Zirconium metal-organic framework (UiO-66) as a robust catalyst toward OSOlvent-free synthesis of remarkable heterocyclic rings, ChemistrySelect 2 (2017) 11906–11911.
[23] Q. Wang, D. Astruc, State of the art and prospects in metal–organic framework (MOF)-Based and MOF-derived nanocatalysis, Chem. Rev. 120 (2019) 1438–1511.
[24] Ltl Nguyen, kka Le, Nts Phan, A zeolite imidazolate framework ZIF-8 catalyst for friedel-crafts acylation, Chin. J. Catal. 33 (2012) 688–696.
[25] U.P. TranK, K. Le, N.T. Phan, Expanding applications of metal− organic frameworks: zeolite imidazolate framework ZIF-8 as an efficient heterogeneous catalyst for the knoevenagel reaction, ACS Catal. 1 (2011) 120–127.
[26] T. Truong, T.M. Hoang, C.K. Nguyen, Q.T. Huynh, N.T. Phan, Expanding applications of zeolite imidazolate frameworks in catalysis: synthesis of quinazolines using ZIF-67 as an efficient heterogeneous catalyst, RSC Adv. 5 (2015) 24769–24776.
[27] M. Hu, S. Zhao, S. Liu, C. Chen, W. Chen, W. Zhu, Y. Li, MOF-Confined sub-2 nm atomically ordered intermetallic PdZn nanoparticles as high-performance catalysts for selective hydrogenation of acetylene, Adv. Mater. 30 (2018) 1801878.
[28] A.M. Omer, E.M. Abd El-Monaem, M.M. Abd El-Latif, G.M. El-Subruiti, A.S. Eltaweil, Facile fabrication of novel magnetic ZIF-67 MOF@aminated chitosan composite beads for the adsorptive removal of Cr(VI) from aqueous solutions, Carbohydr. Polym. 265 (2021) 118084.
[29] Y. Qiao, N. He, X. ZhangX, Zhao, X. Zhao, W. Li, C. Li, In situ growth of MOF crystals to synthesize a graphene oxide/ZIF-7 gel with enhanced adsorption capacity for methylene blue, New J. Chem. 46 (2022) 14103–14111.
[30] L. Valencia, H.N. Abdelhamid, Nanocellulose leaf-like zeolitic imidazolate framework (ZIF-L) foams for selective capture of carbon dioxide, Carbohydr. Polym. 213 (2019) 338–345.
[31] M.A. Ghasemzadeh, Synthesis and characterization of Fe_3O_4@SiO_2 NPs as an effective catalyst for the synthesis of tetrahydrobenzo [a] xanthen-11-ones, Acta Chim. Slov. 62 (2015) 977–985.
[32] M.A. Ghasemzadeh, B. Mirhosseini-Eshkevari, M.H. Abdollahi-Basir, Rapid and efficient one-pot synthesis of 3,4-dihydroquinoxalin-2-amine derivatives catalyzed by Co_3O_4@SiO_2 core-shell nanoparticles under ultrasound irradiation, Comb. Chem. High Throughput Screen. 19 (2016) 592–601.
[33] J. Govan, Y. Gun'ko, Recent advances in the application of magnetic nanoparticles as a support for homogeneous catalysts, Nanomaterials 4 (2014) 222–241.
[34] H. Wang, Y. Wang, A. Jia, C. Wang, L. Wu, Y. Yang, Y. Wang, A novel bifunctional Pd–ZIF-8/rGO catalyst with spatially separated active sites for the tandem Knoevenagel condensation–reduction reaction, Catal. Sci. Technol. 7 (2017) 5572–5584.
[35] M.H. Abdollahi-Basir, F. Shirini, H. Tajik, M.A. Ghasemzadeh, One-pot synthesis of chromenes in the presence of magnetic nanocomposite based on NH_2-UiO-66 (Zr), graphene oxide and Fe_3O_4, J. Mol. Struct. 1263 (2022) 133022.
[36] M. Esmati, B. Zeynizadeh, Synthesis of GO and rGO@Fe3O4@Ni as remarkable nanocatalyst systems for solvent-free and chemoselective coupling reactions of dimedone with aromatic aldehydes, Appl. Organomet. Chem. 35 (2021) e6321–e6338.
[37] A. Ghorbani-Choghamarani, Z. Taherinia, M. Mohammadi, Facile synthesis of Fe3O4@GlcA@Ni-MOF composites as environmentally green catalyst in organic reactions, Environ. Technol. Innov. 24 (2021) 102050–102061.
[38] L. Wang, S. Yang, L. Chen, S. Yuan, Q. Chen, M.Y. He, Z.H. Zhang, Magnetically recyclable Cu-BTC@Fe3O4 composite-catalyzed C(aryl)-S-P bond formation using aniline, P(O)H compounds and sulfur powder, Catal. Sci. Technol. 7 (2017) 2356–2361.

[39] Z. Miao, X. Shu, D. Ramella, Synthesis of a Fe3O4@P4VP@metal-organic framework core-shell structure and studies of its aerobic oxidation reactivity, RSC Adv. (7) (2017) 2773–2779.
[40] Q. Li, S. Jiang, S. Ji, D. Shi, H. Li, Synthesis of magnetically recyclable MOF-5@SiO2@Fe3O4 catalysts and their catalytic performance of Friedel-Crafts alkylation, J. Porous Mater. (22) (2015) 1205–1214.
[41] P. Flatamico, J. Smith, Escherichia coli infections, in: H. Riemann, D. Cliver (Eds.), Food Infection and Intoxication, Elsevier Inc., 2006, pp. 205–239.
[42] M. Schmitt, U. Schuler-Schmid, W. Scmidt-Lorenz, Temperature limits of growth, TNase and enterotoxin production of Staphylococcus aureus strains isolated from foods, Int. J. Food Microbiol. (11) (1990) 1–19.
[43] S. Rostamnia, E. Doustkhah, B. Zeynizadeh, Exfoliation effect of PEG-type surfactant on Pd supported GO (SE-Pd(nanoparticle)/GO) in cascade synthesis of amides: a comparison with Pd(nanoparticle)/rGO, J. Mol. Catal. Chem. 416 (2016) 88–95.
[44] S. Rostamnia, B. Zeynizadeh, E. Doustkhah, H. Golchin Hosseini, Exfoliated Pd decorated graphene oxide nanosheets (PdNP-GO/P123): non-toxic, ligandless and recyclable in greener Hiyama cross-coupling reaction, J. Colloid Interface Sci. 451 (2015) 46–52.
[45] L. Moradi, H. Sadeghi, Efficient pathway for the synthesis of amido alkyl derivatives using KCC-1/PMA immobilized on magnetic MnO2 nanowires as recyclable solid acid catalyst, J. Mol. Struct. 1274 (2023) 134477–134478.
[46] H. Karimi-Maleh, Y. Liu, Z. Li, R. Darabi, Y. Orooji, C. Karaman, F. Karimi, M. Baghayeri, J. Rouhi, L. Fu, S. Rostamnia, S. Rajendran, A.L. Sanati, H. Sadeghifar, M. Ghalkhani, Calf thymus ds-DNA intercalation with pendimethalin herbicide at the surface of ZIF-8/Co/rGO/C3N4/ds-DNA/SPCE; A bio-sensing approach for pendimethalin quantification confirmed by molecular docking study, Chemosphere 332 (2023) 138815–138825.
[47] S. Sadeghi, H. Neamani, L. Moradi, Immobilization of CdCl2on filamentous silica nanoparticles as an efficient catalyst for the solvent free synthesis of some amidoalkyl derivatives, Polycycl. Aromat. Comp. 43 (2022) 1957–1973.
[48] S. Rostamnia, K. Lamei, Diketene-based neat four-component synthesis of the dihydropyrimidinones and dihydropyridine backbones using silica sulfuric acid (SSA), Chin. Chem. Lett. 23 (2012) 930–932.
[49] P.P. Upare, D.-Y. Hong, J. Kwak, M. Lee, S.K. Chitale, J.-S. Chang, D.W. Hwang, Y. K Hwang, Direct chemical conversion of xylan into furfural over sulfonated graphene oxide, Catal. Today 324 (2019) 66–72.
[50] W.S. Hummers Jr., R.E. Offeman, Preparation of graphitic oxide, J. Am. Chem. Soc. 80 (1958), 1339-1339.
[51] S. Sanaei-Rad, M.A. Ghasemzadeh, S. Aghaei, Synthesis and structure elucidation of $ZnFe_2O_4$/IRMOF-3/GO for the drug delivery of tetracycline and evaluation of their antibacterial activities, J. Organomet. Chem. 960 (2022) 122–221.
[52] P. Peizhi Guo, Lijun Cui, Yiqian Wang, Meng Lv, Baoyan Wang, X.S. Zhao, Facile synthesis of ZnFe2O4 nanoparticles with tunable magnetic and sensing properties, Langmuir 29 (2013) 899–9003.
[53] P.A. Vinosha, L.A. Mely, J.E. Jeronsia, S. Krishnan, S.J. Das, Synthesis and properties of spinel $ZnFe_2O_4$ nanoparticles by facile co-precipitation route, Optik 134 (2017) 99–108.
[54] J. Shi, L. Zhang, N. Sun, D. Hu, Q. Shen, F. Mao, Q. Gao, W. Wei, Facile and rapid preparation of Ag@ZIF-8 for carboxylation of terminal alkynes with CO_2 in mild conditions, ACS Appl. Mater. Interfaces 11 (2019) 28858–28867.
[55] C. Adhikari, A. Das, A. ChakrabortyZeolitic, Imidazole framework (ZIF) nanospheres for easy encapsulation and controlled release of an anticancer drug doxorubicin under different external stimuli: a way toward smart drug delivery system, Mol. Pharm. 12 (2015) 3158–3166.
[56] A.A. El-Bindary, E.A. Toson, K.R. Shoueir, H.A. Aljohani, M.M. Abo-Ser, Metal-organic frameworks as efficient materials for drug delivery: synthesis, characterization, antioxidant, anticancer, antibacterial and molecular docking investigation, Appl. Organomet. Chem. 34 (2020) e5905–e5919.
[57] M. Hasanzadeh, N. Shadjou, (Fe_3O_4)-Graphene oxide-OSO_3H as a new magnetic nanocatalyst for electro-oxidation and determination of selected parabens, J. Nanosci. Nanotechnol. 13 (2013) 4909–4916.
[58] Y. Wei, Z. Hao, F. Zhang, H. Li, A functionalized graphene oxide and nano-zeolitic imidazolate framework composite as a highly active and reusable catalyst for [3 + 3] formal cycloaddition reactions, J. Mater. Chem. 3 (2015) 14779–14785.
[59] D. Huang, Q. Xin, Y. Ni, Y. Shuai, S. Wang, Y. Li, H. Ye, L. Lin X, Ding, Y. Zhang, Synergistic effects of zeolite imidazole framework@graphene oxide composites in humidified mixed matrix membranes on CO2 separation, RSC Adv. 8 (2018) 6099–6109.
[60] S. Sanaei-Rad, M.A. Ghasemzadeh, S.M.H. Razavian, Synthesis of a novel ternary ZIF-8/GO/$MgFe_2O_4$ nanocomposite and its application in drug delivery, Sci. Rep. 11 (2021) 18734.
[61] A.R. Abbasian, M. Shafiee Afarani, One-step solution combustion synthesis and characterization of $ZnFe_2O_4$ and ZnFe1.6O4 nanoparticles, Appl. Phys. 125 (2019) 721.
[62] C. Shuai, Y. Xu, P. Feng, G. Wang, S. Xiong, S. Peng, Antibacterial polymer scaffold based on meOSOporous bioactive glass loaded with in situ grown silver, Chem. Eng. J. 374 (2019) 304–315.
[63] D.R. Dreyer, S. Park, C.W. Bielawski, R.S. Ruoff, The chemistry of graphene oxide, Chem. Soc. Rev. 39 (2010) 228–240.
[64] E. Doustkhah, S. Rostamnia, Covalently bonded sulfonic acid magnetic graphene oxide: Fe3O4@GO-Pr-OSO_3H as a powerful hybrid catalyst for synthesis of indazolophthalazinetriones, J. Colloid Interface Sci. 478 (2016) 280–287.
[65] H. Su, Z. Li, Q. Huo, J. Guan, Q. Kan, Immobilization of transition metal (Fe2+, Co2+, VO2+ or Cu2+) Schiff base complexes onto graphene oxide as efficient and recyclable catalysts for epoxidation of styrene, RSC Adv. 4 (2014) 9990–9996.
[66] N. Uregen, K. Pehlivanoğlu, Y. Ozdemir, Y. Devrim, Development of polybenzimidazole/graphene oxide composite membranes for high-temperature PEM fuel cells, Int. J. Hydrogen Energy 42 (2018) 2636–2647.
[67] N. Esmaeili, P. Mohammadi, M. Abbaszadeh, H. Sheibani, Au nanoparticles decorated on magnetic nanocomposite (GO-Fe_3O_4/Dop/Au) as a recoverable catalyst for degradation of methylene blue and methyl orange in water, Int. J. Hydrogen Energy 44 (2019) 23002–23009.
[68] P.P. Warekar, G.B. Kolekar, M.B. Deshmukh, P.V. Anbhule, An efficient and modified biginelli-type synthesis of 3,4-dihydro-1H-indeno[1,2-d]pyrimidine-2,5-dione using phosphorous pentoxide, Synth. Commun. 44 (2014) 3594–3601.
[69] K. Aswin, S.S. Mansoor, K. Logaiya, P.N. Sudhan, R.N. Ahmed, Facile synthesis of 3,4-dihydropyrimidin-2(1H)-ones and -thiones and indeno[1,2-d]pyrimidines catalyzed byp-dodecylbenzenesulfonic acid, J. Taibah Univ. Sci. 8 (2014) 236–247.
[70] V.V. Dabholkar, S.R. Patil, R.V. Pandey, Design, synthesis, characterization, and antimicrobial activity of biginelli products of indandione, J. Heterocycl. Chem. 49 (2012) 929–932.
[71] J. Park, K. An, Y. Hwang, J.G. Park, H.J. Noh, Y. J, J.H. Kim, N.M. Park, T. Hyeon Hwang, Ultra-large-scale syntheses of monodisperse nanocrystals, Nat. Mater. 3 (2004) 891–895.
[72] M. Aguirre-Díaz, L. Gándara, F. Iglesias, M. Snejko, N. Gutiérrez-Puebla, E. Ángeles Monge, Tunable catalytic activity of solid solution metal-organic frameworks in one-pot multicomponent reactions, J. Am. Chem. Soc. 137 (2015), 6132-1635.